

Size dependent tunneling and optical spectroscopy of CdSe quantum rods

David Katz, Tommer Wizansky, and Oded Millo*

*Racah Institute for Physics, and the Center for Nanoscience and Nanotechnology,
The Hebrew University of Jerusalem, Jerusalem 91904, Israel*

Eli Rothenberg, Taleb Mokari, and Uri Banin†

*Institute of Chemistry, and the Center for Nanoscience and Nanotechnology,
The Hebrew University of Jerusalem, Jerusalem 91904, Israel*

Photoluminescence excitation spectroscopy and scanning tunneling spectroscopy are used to study the electronic states in CdSe quantum rods that manifest a transition from a zero dimensional to a one dimensional quantum confined structure. Both optical and tunneling spectra show that the level structure depends primarily on the rod diameter and not on length. With increasing diameter, the band-gap and the excited state level spacings shift to the red. The level structure was assigned using a multi-band effective-mass model, showing a similar dependence on rod dimensions.

PACS numbers: 73.22.-f, 73.63.-b, 78.67.-n

Colloidal semiconductor nanocrystals are a class of nanomaterials that manifest the transition from the molecular limit to the solid state [1, 2], with significant potential for serving as building blocks of nano-devices in applications ranging from lasers [3, 4] and opto-electronic devices [5] to biological fluorescence tagging [6]. Shape control of such colloiddally prepared nanostructures has been recently achieved by modifying the synthesis to obtain rod shaped particles - quantum rods [7]. Quantum rods (QRs) exhibit electronic and optical properties different than QDs. For example, unlike the spherical dots, QRs have linearly polarized emission as demonstrated recently by fluorescence measurements on single rods [8], leading to polarized lasing [4]. In this letter we combine optical and tunneling spectroscopies to investigate the electronic level structure of CdSe quantum rods, and study its dependence on rod length and diameter. The levels are assigned with the use of a multi-band effective-mass model. The study provides significant insight on the evolution of the electronic structure from zero dimensional QDs to one-dimensional quantum wires.

The combination of scanning tunneling spectroscopy with PLE has proven to be a powerful approach to decipher the level structure of nanocrystal QDs [2, 9]. While in the optical spectra, allowed valence band (VB) to conduction band (CB) transitions are detected [10, 11], in tunneling spectroscopy the CB and VB states can be separately probed yielding complimentary information on the level structure [9, 12, 13, 14]. These data provide an important benchmark for testing theoretical models developed for describing the level structure in strongly quantum-confined nanostructures. This was demonstrated for spherical nanocrystal QDs where multi-band effective mass approaches [10, 11, 15] and atomistic pseudo-potential theory [16] were both used to describe measured size-dependent level structure. In a recent work by Hu et al. [17], the pseudo-potential approach was also applied for the calculation of energy levels in

rods of small diameter and aspect ratios up to six.

The CdSe system studied here is highly developed synthetically, to a level where it serves as a model system for colloidal semiconductor nanostructures. Fig. 1 presents transmission electron microscopy (TEM) images of typical samples of CdSe quantum rods grown using the well developed methods of colloidal nanocrystal synthesis [7, 18, 19]. For the study of length and diameter dependence we prepared six different samples with dimensions that can be divided into two groups- three samples with radii ~ 1.8 nm and lengths ranging from 11 to 31 nm, and three samples, with radii ~ 3.2 nm and lengths ranging from 11 to 60 nm. For the low temperature optical experiments, optically clear free-standing polymer films containing the rods were prepared. The cooled samples showed absorption spectra with several transitions and had a distinct photoluminescence (PL) peak assigned to band-gap emission. The positions of the absorption onset and PL peak red shifted with increasing diameter and showed no significant variation with rod length [Fig. 4(a)] [20].

The PLE spectra presented in Fig. 1, measured on four samples, were obtained by opening a narrow detection window at the blue edge of the inhomogeneously broadened PL peak [10, 11]. The spectra are less structured as compared with those measured on QDs due to the increased sources of inhomogeneous broadening in rods and due to the intrinsically less discrete level structure. A striking feature is the nearly identical level structure observed for the two QR samples of small diameter (traces a,b), which differs significantly from the spectra measured on the thicker rods (traces c,d), although in each group the aspect ratios vary from 3 to about 10. This shows clearly that not only the band-gap of the rods depends mainly on the diameter, but also the excited optical transitions.

The optical measurements were accompanied by tunneling measurements performed at 4.2 K on *single* QRs

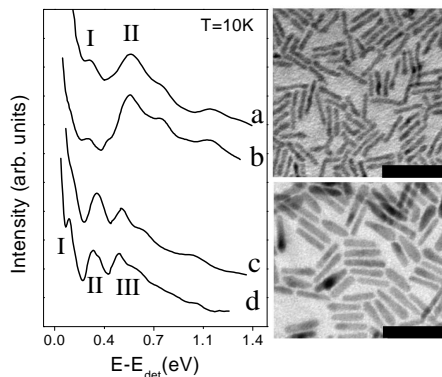


FIG. 1: PLE spectra for CdSe QRs are shown in the left frame (a) 31×1.9 (length times radius) nm, $E_{det} = 2.25$ eV (b) 11×1.6 nm, $E_{det} = 2.25$ eV (c) 60×3.3 nm, $E_{det} = 2.00$ eV (d) 11×2.9 nm, $E_{det} = 2.03$ eV, with the zero energy representing the position of the detection window, E_{det} . Relevant optical transitions are marked. The structure above 0.7 eV is overlapping peaks of the excitation lamp that could not be completely normalized out. TEM images of two QR samples, 31×3.9 nm (top), and 30×3.2 nm (bottom), are shown in the right. Scale bar is 50 nm.

deposited on graphite, using a cryogenic scanning tunneling microscope (STM) [14]. A topographic image of a nanorod 25 nm in length and 2 nm in radius is presented in Fig. 2(a). After identifying such an isolated QR, tunneling dI/dV vs. V spectra were obtained in a double barrier tunnel junction (DBTJ) configuration [9, 12, 13, 14], as shown schematically in Fig. 2(b). The spectra were measured with the tip retracted from the QR to a distance where the bias voltage is dropped largely across the tip-QR junction, and charging effects are avoided. As a result, CB (VB) states appear at positive (negative) sample bias, and the peak separations are close to the real QR level spacings. Hence, the dI/dV spectra yield direct information on the QR level spectrum [12, 13, 14].

The tunneling spectra in Fig. 2(c) further demonstrate, in accordance with the PLE data, that the QR level structure depends primarily on the diameter of the QRs, not on their length. Most significantly, the region of suppressed tunneling conductance (null density of states) around zero bias, associated with the quasi-particle energy gap, is red shifted upon QR thickening, from ~ 2.4 eV in the upper two curves ($r \sim 2$ nm) to ~ 2.2 eV in the lower curves ($r \sim 2.7$ nm). This trend was not observed as clearly for the spacing between the CB ground state (CB1) and the first excited state (CB2), as evident also from Fig. 4(b). Level CB3 appearing in the lower trace was observed in $\sim 50\%$ of the measurements, where the current did not reach the saturation limit before resolving this level. The VB is considerably more dense and complex (see below) and its level structure was not reliably resolved in our tunneling spectra; we thus only denote

the first (ground state) peak as VB1 [Fig. 2(c)]. More insight into the QR level structure, including the excited VB levels, is gained by correlating the tunneling spectra with allowed optical VB to CB transitions and comparing these data with model level-structure calculations.

To calculate the electronic structure of the rods we employ the formalism developed by Sercel and Vahala for quantum wires [21]. Similar basis functions were used for the envelope wavefunctions, with quantum numbers reflecting the cylindrical symmetry of the QR: n , the principal number (associated with the number of nodes along the radius), and F_z and L_z , the projections of the total and the envelope angular momenta along the z (symmetry) axis, respectively. Here, $F_z = J_z + L_z$, where J_z is the projection of band-edge Bloch angular momentum along the z axis. The finite length L of the QRs is expressed by introducing an additional quantum number, denoted by m , and a related factor, $\exp(i\pi m z/L)$, to the envelope wavefunctions, replacing the continuum wavevector K_z in Ref. 21.

We first consider the CB level structure. Here, due to the large band-gap of CdSe (1.84 eV), the uncoupled one-band effective-mass model with quantum numbers (n, L_z, m) is adequate for rods of large enough aspect ratio [17, 21]. Figure 3(a) presents CB energy levels calculated using this model for a particle in a finite cylindrical potential-well ($U = 5$ eV), as a function of radius and length (inset). The CB states with $L_z = 0, 1$, and 2 are denoted CB1, CB2 and CB3, respectively. This figure clearly depicts the strong dependence of the energy levels on the QR radius, due to the strong confinement associated with this 'narrow dimension', as opposed to the near lack of length dependence shown in the upper inset. The length dependence becomes significant only for small aspect ratio (around 2), or for high m values, effectively shortening the QR, since the number of nodes along the z axis is $m - 1$, in agreement with Ref. 17.

The VB states were calculated using the four-band effective-mass model that couples heavy and light holes [21], where the quantum numbers are now (n, F_z, m) . Results of this calculation, performed for an infinite cylindrical potential-well, are presented in Fig. 3(b), where states with $F_z = 1/2, 3/2$, and $5/2$ (and $m = 1$) are shown. Again, the near lack of dependence of the level structure on the rod length is manifested by the inset. It is evident that the VB is significantly more dense as compared to the CB. Yet, the VB levels near the band-edge can be divided into three groups: VB1, denoting the two upper levels, VB2, the three subsequent ones and VB3, the next group. Each of these groups is composed of various F_z levels, where, in turn, each F_z level has contributions from both heavy and light holes ($J_z = 3/2$ and $1/2$, respectively), and thus from wavefunctions of different L_z values. This VB mixing leads to very weak selection rules for the optical transitions.

In Fig. 4 we compare the measured optical transi-

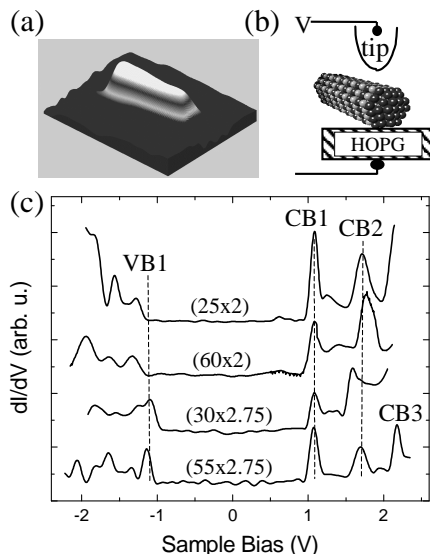


FIG. 2: (a) STM image of a QR 25 nm long and 2 nm in radius. (b) Schematic of the DBTJ configuration used for acquiring the tunneling spectra. (c) $dI/dV - V$ tunneling spectra for QRs of various lengths and radii, marked above each curve in nm. For clarity, the spectra were shifted horizontally to align the CB1 peaks. The vertical dashed lines are guides to the eye. The tunneling set values were in the range $V_s = 1.5 - 2$ eV and $I_s = 50 - 80$ pA.

tions and tunneling spectra with our theoretical calculations. The gap extracted from the optical measurements (solid circles) and the gap identified in the tunneling data (empty circles), are plotted in Fig. 4(a) along with the calculated energy gap, VB1-CB1. In order to compare with the quasi-particle (tunneling) gap, the measured excitonic (optical) gap was corrected for the electron-hole Coulomb interaction. As a first approximation, we modified the expression given in Ref. 10 for QDs, $1.8e^2/kr$ (where k is the dielectric constant), to take into account the fact that in our QRs strong confinement holds only for the radial dimension. We thus replace the radius, r , by $(r^2 a_o)^{1/3}$, where a_o is the Bohr radius, 5.7 nm. A relatively good agreement between the calculated and measured energy gaps is found, for both tunneling and optical experiments. However, the tunneling gaps are higher in energy and show a stronger dependence on radius as compared to the optical data, as was previously observed for QDs [9, 10, 11]. This can be ascribed to the non-vanishing voltage drop on the QR-substrate junction [12, 13, 14] and on the uncertainty involved in the determination of the QR radii [9]. Concerning the optical gap, the transition from both $F_z = 1/2$ and $3/2$ VB1 states are allowed. In the absorption they are too close to be resolved, but we note that the state with $F_z = 1/2$ is the top-most state, from which theory predicts a transition polarized along the symmetry axis [22], consistent with PL polarization measurements for QRs [8].

Turning now to the excited levels, Fig. 4(b) shows spacings of the PLE transitions I and II with respect to the band-gap transition, together with levels CB2 and CB3 measured with respect to CB1, detected by tunneling. The data are presented as a function of the band-gap measured in each experiment, thus eliminating the possible problem of QR radius estimation mentioned above. Most interesting is the good agreement of the spacing between PLE transition II and the band-gap transition (solid squares) with the tunneling data for the CB2-CB1 level separation (open squares), allowing a clear assignment of optical transition II. Both the optical and tunneling data correlate with the theoretical curve for the CB2-CB1 spacing. It is also clear now that PLE transition I (solid stars) can only take place between an excited VB state and the CB ground state. However, due to the intricate VB level structure and the broad PLE features, it cannot be unambiguously assigned, and relatively good agreement is found for both calculated VB2-VB1 and VB3-VB1 level spacing (dashed lines). Transition III was resolved only for the three samples with larger diameters, and thus cannot be assigned. Considering again the tunneling data, Fig. 4(b) shows a weaker size (energy-gap) dependence for CB2 and CB3 as compared to theory. This may be partly due to our over-simplified model, where we assume a sharp (square-well) and somewhat large (5 eV) confining potential. These approximations should affect mainly the higher levels.

The contribution of high m states was not clearly resolved in our spectra. In the PLE data, such a contribution possibly manifests itself in the broadening of the peaks, as compared with QDs. As for the tunneling spectra, due to the small wavevector component parallel to the surface associated with the tunneling electron, coupling to higher m values may be suppressed. We note, however, that our spectra often exhibit a broad background on top of which the peaks are superimposed (e.g., the middle curves in Fig. 2).

In conclusion, optical and tunneling spectroscopic data for CdSe QRs show that the level structure is dominated by radius rather than by the length. This behavior, manifested also in the theoretical calculations, reveals the quasi one-dimensional nature of the QR even for aspect ratios as small as three. This allows one to select a desired QR length and tune its optical or electrical properties at will, using the diameter. This ability is of significant importance for future nanotechnology applications of QRs [4, 23].

This work was supported in parts by the US-Israel Binational Foundation, the DIP foundation and by the Israel Science Foundation.

* Electronic address: milode@vms.huji.ac.il

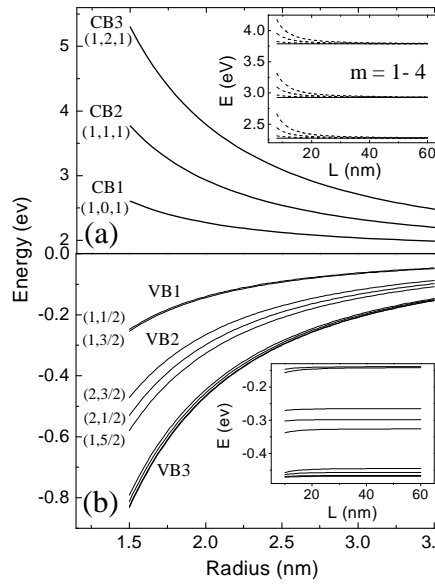


FIG. 3: Calculated energy levels of CdSe QRs. (a) CB states versus nanorod radius, for a 30 nm long quantum numbers (n, L_z, m) are denoted. (b) The levels versus QR radius calculated for a 30 nm long quantum numbers (n, F_z) are denoted ($m = 1$). (consists of states with $F_z = 1/2, 3/2, 5/2,$ and 7 Length dependence for the respective energy levels nm in radius. The upper inset shows also the dep the m quantum number. The energies are given w to the bulk VB edge. Effective masses for electron and the bulk energy gap were taken from Ref. 15.

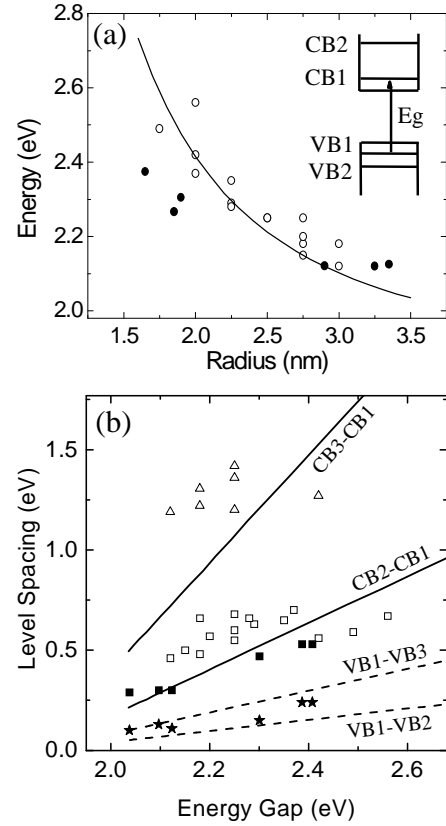


FIG. 4: (a) Energy gap versus QR radius. The tunneling data (empty circles) and the theory (solid line) represent the energy separations VB1-CB1 (see Figs. 2 and 3). The optical data (solid circles) were determined from the first absorption peak and corrected for the electron-hole Coulomb interaction, see text. The inset illustrates the relevant optical transition from VB1 to CB1. (b) Excited energy states versus energy gap. The calculated energy level separations, as denoted, are depicted in the solid and dashed lines. The respective separations between the tunneling peaks are denoted by open symbols. Spacing between PLE transitions I and II and the optical energy gap are presented by solid stars and squares, respectively. For the optical data, the energy gap was taken as the detection window corrected for the electron-hole Coulomb interaction.

[†] Electronic address: banin@chem.ch.huji.ac.il
 [1] A. P. Alivisatos, *Science* **271**, 933 (1996).
 [2] O. Millo, D. Katz, Y. W. Cao, and U. Banin, *Lett.* **86**, 5751 (2001).
 [3] V. Klimov et al., *Science* **290**, 314 (2000).
 [4] M. Kazes et al., *Adv. Materials* **14**, 317 (2002).
 [5] N. Tessler, V. Medvedev, M. Kazes, S. H. U. Banin, *Science* **295**, 1506 (2002).
 [6] M. Bruchez et al., *Science* **281**, 2013 (1998).
 [7] X. G. Peng et al., *Nature* **404**, 59 (2000).
 [8] J. T. Hu et al., *Science* **292**, 2060 (2001).
 [9] U. Banin, Y. W. Cao, D. Katz, and O. Mi **400**, 542 (1999).
 [10] D. J. Norris and M. G. Bawendi, *Phys. Rev. E* (1996).
 [11] U. Banin et al., *J. Chem. Phys.* **109**, 2306 (1998).
 [12] E. P. A. M. Bakkers and D. Vanmaekelbergh, *B* **62**, R7743 (2000).
 [13] E. P. A. M. Bakkers et al., *Nano Lett.* **1**, 551 (2001).
 [14] D. Katz, O. Millo, S. H. Kan, and U. Banin, *Lett.* **79**, 117 (2001).
 [15] A. I. Ekimov et al., *J. Op. Soc. Am. B* **10**, 10 (1993).
 [16] H. X. Fu and A. Zunger, *Phys. Rev. B* **57**, R15 (1998).
 [17] J. T. Hu et al., *J. Phys. Chem.* **106**, 2447 (2002).
 [18] L. Manna, E. C. Scher, and A. P. Alivisatos, *Science* **297**, 1212 (2002).

[20] L. S. Li, J. T. Hu, W. D. Yang, and A. P. Alivisatos, *Nano Lett.* **1**, 349 (2001).
 [21] P. C. Sercel and K. J. Vahala, *Phys. Rev. B* **42**, 3690 (1990).
 [22] P. C. Sercel and K. J. Vahala, *Phys. Rev. B* **44**, 5681 (1991).
 [23] W. U. Huynh, J. J. Dittmer, and A. P. Alivisatos, *Science* **295**, 2425 (2002).